Protein Science (2000), *9*:1743–1752. Cambridge University Press. Printed in the USA.

Structure of a (Cys_3His) zinc ribbon, a ubiquitous motif in archaeal and eucaryal transcription

HUNG-TA CHEN,[1,2] PASCALE LEGAULT,[3] JOHN GLUSHKA,[4] JAMES G. OMICHINSKI,[2,3] AND ROBERT A. SCOTT[1,2,3]

[1]Center for Metalloenzyme Studies, Chemistry Building, University of Georgia, Athens, Georgia 30602-2556
[2]Department of Chemistry, Chemistry Building, University of Georgia, Athens, Georgia 30602-2556
[3]Department of Biochemistry and Molecular Biology, Life Sciences Building, University of Georgia, Athens, Georgia 30602-7229
[4]Complex Carbohydrate Research Center, 220 Riverbend Road, University of Georgia, Athens, Georgia 30602-4712

(RECEIVED February 10, 2000; FINAL REVISION June 15, 2000; ACCEPTED June 30, 2000)

Abstract

Transcription factor IIB (TFIIB) is an essential component in the formation of the transcription initiation complex in eucaryal and archaeal transcription. TFIIB interacts with a promoter complex containing the TATA-binding protein (TBP) to facilitate interaction with RNA polymerase II (RNA pol II) and the associated transcription factor IIF (TFIIF). TFIIB contains a zinc-binding motif near the N-terminus that is directly involved in the interaction with RNA pol II/TFIIF and plays a crucial role in selecting the transcription initiation site. The solution structure of the N-terminal residues 2–59 of human TFIIB was determined by multidimensional NMR spectroscopy. The structure consists of a nearly tetrahedral $Zn(Cys)_3(His)_1$ site confined by type I and "rubredoxin" turns, three antiparallel β-strands, and disordered loops. The structure is similar to the reported zinc-ribbon motifs in several transcription-related proteins from archaea and eucarya, including *Pyrococcus furiosus* transcription factor B (*Pf*TFB), human and yeast transcription factor IIS (TFIIS), and *Thermococcus celer* RNA polymerase II subunit M (*Tc*RPOM). The zinc-ribbon structure of TFIIB, in conjunction with the biochemical analyses, suggests that residues on the β-sheet are involved in the interaction with RNA pol II/TFIIF, while the zinc-binding site may increase the stability of the β-sheet.

Keywords: human transcription factor IIB; multidimensional NMR; transcription preinitiation complex; zinc ribbon

Transcription initiation of protein-encoding genes in eucarya is mediated by RNA polymerase II (RNA pol II) and a complex array of initiation factors (Orphanides et al., 1996; Hampsey, 1998). The formation of a multiprotein complex, which is referred to as the preinitiation complex (PIC), triggers the transcription process. A minimal set of factors suffices for basal (unregulated) transcription initiation. These so-called basal or general transcription factors (GTFs) include the TBP (TATA-binding protein) subunit of TFIID, TFIIB, TFIIF, TFIIE, TFIIH, along with RNA pol II. In vitro studies using highly purified transcription factors indicate that the formation of the PIC begins with binding of TBP to the TATA element. Subsequent association of TFIIB with TBP facilitates entry of RNA pol II and the associated TFIIF into the complex. Finally, binding of TFIIE and TFIIH yields a PIC that is capable of accurately initiating the synthesis of the RNA chain in the presence of nucleoside triphosphates. This stepwise pathway of PIC assembly has been challenged by recent identification of a RNA pol II holoenzyme, pre-associated with GTFs, from both yeast and mammalian cells (Myer & Young, 1998). This suggests that RNA pol II also binds promoters in vivo as a pre-assembled complex.

In its critical role as the functional (and likely structural) bridge between TBP and RNA pol II, TFIIB utilizes two distinct domains. The N-terminal portion of TFIIB contains a metal-binding sequence Cys-X_2-His/Cys-$X_{15\text{-}17}$-Cys-X_2-Cys that has the potential to form a nonclassical zinc finger-like domain (Pinto et al., 1992). Previously, we reported the NMR-derived solution structure of the metal-binding domain of *Pyrococcus furiosus* TFB that forms a "zinc ribbon" (Zhu et al., 1996). The proteolytically stable C-terminal core domain of TFIIB contains two imperfect direct repeats, conferring two similar cyclin A-like structural domains, each consisting of five α-helices (Bagby et al., 1995; Nikolov et al., 1995). The metal-binding domain and the two imperfect repeats of TFIIB are commonly present in the TFIIBs of eucaryal organisms as well as in the TFBs from archaea. The N- and C-terminal domains engage in an intramolecular interaction that is

Reprint requests to: Robert A. Scott, Department of Chemistry, Chemistry Building, University of Georgia, Athens, Georgia 30602-2556; e-mail: rscott@uga.edu

Abbreviations: DQF-COSY, double-quantum-filtered correlation spectroscopy; FPLC, fast protein liquid chromatography; HSQC, heteronuclear single-quantum coherence; hTFIIB-NTD, the N-terminal domain of human transcription factor IIB; hTFIIS-CTD, the C-terminal domain of human transcription factor IIS; NOE, nuclear Overhauser effect; NOESY, NOE spectroscopy; *Pf*TFB-NTD, the N-terminal domain of *Pyrococcus furiosus* transcription factor B; RMSD, root-mean-square deviation; TOCSY, total correlation spectroscopy.

disrupted by activators, facilitating assembly of the PIC (Roberts & Green, 1994). The C-terminal region binds to the TBP–TATA element complex as demonstrated by the crystal structure of the ternary complex containing TBP, TATA-element, and the C-terminal domain of TFIIB (TFIIB-CTD) (Nikolov et al., 1995). The N-terminal region of TFIIB plays an essential role in RNA pol II recruitment and in RNA pol II start site selection (Barberis et al., 1993; Buratowski & Zhou, 1993; Hisatake et al., 1993). Mutations within or deletion of the metal-binding domain significantly compromise the ability of TFIIB to recruit RNA pol II-TFIIF into the initiation complex. Mutations in the N-terminal region of TFIIB also alter RNA pol II start sites in yeast and humans (Pinto et al., 1994; Pardee et al., 1998; Hawkes & Roberts, 1999; Wu & Hampsey, 1999), suggesting a role for TFIIB as a precise spacer between TBP and RNA pol II on the promoter in determining the transcription start site.

The C(H/C)CC metal-binding motif (zinc ribbon) is highly conserved among eucaryal and archaeal TF(II)Bs. Definitive identification of the physiologically relevant metal used by TF(II)B is not available, although the most likely candidate is zinc. Heterologous expression allows incorporation of Fe, Co, and other metals into the C(H/C)CC motif and the metal-binding site bears significant structural resemblance to the rubredoxin site, which binds Fe. Sequence homologs of this motif are also found in several proteins involved in transcription, including TFIIS (Qian et al., 1993; Olmsted et al., 1998), RNA pol II subunits (Qian et al., 1993; Wang et al., 1998; Cramer et al., 2000), and TFIIE (Ohkuma et al., 1991; Peterson et al., 1991). In our continuing efforts to characterize the assembly and topology of the archaeal PIC, we are using biophysical and structural biology tools to compare components of the eucaryal and archaeal PICs. Here we report the NMR-based structure of hTFIIB-NTD, a protein fragment consisting of the N-terminal 59 residues of human TFIIB. The results illustrate that the metal-binding CHCC motif of TFIIBs in higher eucarya also forms the basic zinc-ribbon fold as observed in the CCCC motif of the archaeal homolog.

Results

Spectral assignments and secondary structure determination

Sequence-specific assignment of ^{1}H and ^{15}N resonances was achieved through correlations from two-dimensional (2D) ^{1}H-^{1}H NOESY, ^{1}H-^{15}N HSQC, and three-dimensional (3D) ^{15}N-edited NOESY-HSQC spectra using well-established strategies (Wüthrich, 1986; Clore & Gronenborn, 1989). Sequential H^N-H^N or H^α-H^N NOE connectivities are not observed for residues Ala2–Thr4 and Ser56–Lys59, and consequently, no NMR assignments were made for these residues. Side-chain ^{1}H resonances were assigned from ^{1}H DQF-COSY, ^{1}H TOCSY, and ^{1}H-^{15}N HSQC-TOCSY spectra.

Elements of secondary structure were identified on the basis of cross-peak patterns and intensities observed in ^{1}H NOESY and ^{1}H-^{15}N NOESY-HSQC spectra. Interresidue NOE connectivities are summarized in the NOE intensity diagram (Fig. 1A). Strong sequential H^α-H^N NOEs were found in residues Ala21–Tyr27, Gly30–Cys34, and Gly38–Gly42 (Fig. 1A), indicating an extended β-strand backbone conformation. Long-range H^α-H^α, H^α-H^N, and H^N-H^N NOE connectivities were observed between residues with the β-strand conformation as indicated in Figure 1B. There are several other residues for which the presence of strong sequential H^α-H^N NOEs suggests β-strand conformation (Fig. 1A), but in these cases the existence of β-sheet cannot be confirmed through the observation of long-range NOE connectivities. Interstrand hydrogen bonds in the β-strands were identified on the basis of NOE connectivities and from the slowly exchanging amide protons determined by observation of remaining amide cross peaks in a series of ^{1}H-^{15}N HSQC experiments collected after dissolution in D_2O. The residues in the three predicted antiparallel β-strands are depicted in Figure 1B, along with sequential and long-range NOE connectivities and interstrand hydrogen bonds.

NOE cross-peak patterns characteristic of a type I turn (Wüthrich, 1986) were found for residues Cys15–His18. The sequential and medium-range ^{1}H-^{1}H NOEs for the type I turn are the strong NOE between Asn17 H^N and His18 H^N, the medium NOE between Pro16 H^δ and Asn17 H^N, the weak NOE between Pro16 H^α and His18 H^N, and the weak NOE between Cys15 H^α and His18 H^N. NOE cross-peak patterns characteristic of a metal-binding "rubredoxin" turn were observed for residues Cys34–Leu39 (Summers et al., 1990; Fourmy et al., 1993; Perez-Alvarado et al., 1994). The NOE cross peaks involved in this turn are the weak NOE between Cys34 H^N and Gly38 H^N, the medium NOE between Cys34 H^N and Leu39 H^N, the strong NOE between Glu36 H^N and Cys37 H^N, the medium NOE between Glu36 H^N and Gly38 H^N, the strong NOE between Cys37 H^N and Gly38 H^N, the medium NOE between Cys37 H^N and Leu39 H^N, and the strong NOE between Gly38 H^N and Leu39 H^N. The presence of several $d_{\alpha N}(i, i + 2)$ NOEs in residues His18–Ala21 and Tyr27–Gly30 also suggest turns. However, the existence of characteristic and stable turns for His18–Ala21 and Tyr27–Gly30 could not be confirmed through the observation of the expected NOE cross-peak patterns.

Identification of the metal-binding mode

A zinc coordination sphere of three sulfurs and one oxygen or nitrogen is suggested by EXAFS studies of the full-length hTFIIB and hTFIIB-NTD proteins (Colangelo et al., 2000). Based on the primary structure of hTFIIB-NTD (Fig. 1A) and the sequence alignment (see below), the residues involved in zinc binding are suggested to be Cys15, His18, Cys34, and Cys37. His18 can coordinate the zinc through either the $N^{\delta 1}$ or the $N^{\epsilon 2}$ atoms. To identify the nitrogen atom coordinating the zinc, a DG/SA calculation was carried out with covalent restraints only from sulfurs in the three cysteines. The structural models generated from the DG/SA calculation indicated unambiguously that the zinc could only coordinate the $N^{\delta 1}$ atom of His18. The evidence for the coordination mode involves strong NOEs between His18 $H^{\epsilon 1}$ and the two Cys37 H^βs, medium NOE between His18 $H^{\epsilon 1}$ and Cys37 H^N, and medium NOE between His18 $H^{\delta 2}$ and His18 H^α. This mode of coordination is also supported by the tautomeric state of the imidazole ring of His18 inferred from the ^{15}N chemical shifts of the $N^{\delta 1}$ (224.4 ppm) and $N^{\epsilon 2}$ (172.1 ppm) nuclei using a 2D long-range ^{1}H-^{15}N HSQC spectrum (data not shown). The ^{15}N chemical shifts of these two nuclei clearly indicate that $N^{\epsilon 2}$ is protonated, while $N^{\delta 1}$ is not (Halkides et al., 1996). The $N^{\delta 1}$ atom of His18 was, therefore, incorporated into the tetrahedral zinc-binding center with appropriate covalent bond restraints in the final structural refinement.

Converged structures and structural description

Twenty-five lowest energy structures were obtained based on a total of 443 experimentally derived distance restraints giving an average of about 15 restraints per residue (Table 1). The coordi-

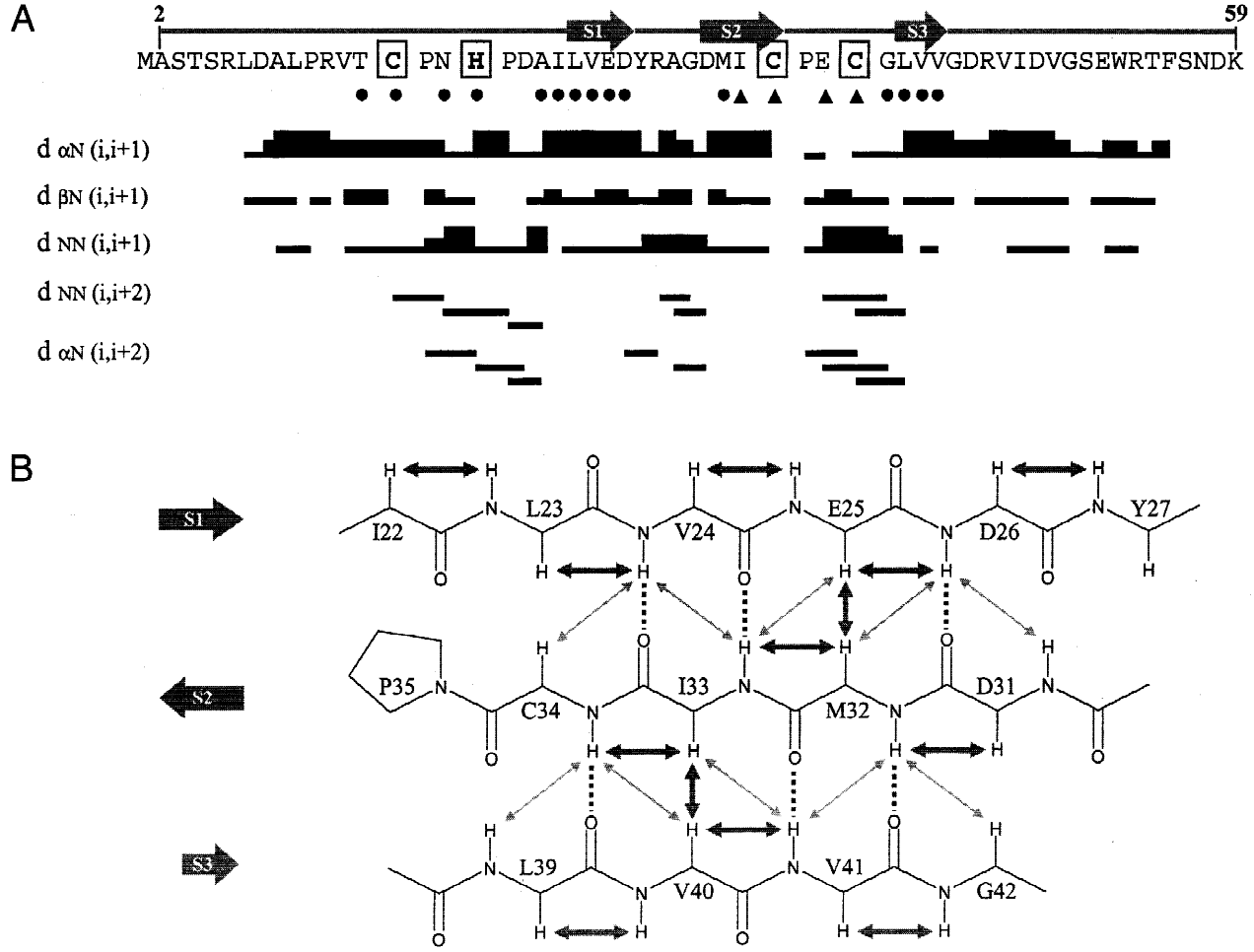

Fig. 1. NOE connectivities and slowly exchanging amide protons. **A:** Sequential and medium-range NOEs are represented by the lines connecting the amino-acid residues. The corresponding amino-acid sequence of hTFIIB-NTD is given at the top. The thickness of the lines denotes the relative intensities of NOE cross peaks. The symbols $d_{NN}(i,j)$, $d_{\alpha N}(i,j)$, and $d_{\beta N}(i,j)$ represent NOE connectivities involving the H^N, H^α, and H^β of residue i and amide protons (H^δ and $H^{\delta'}$ of prolines) of residue j. Filled circles indicate residues that retained amide cross peaks in the HSQC spectrum 30 min after dissolution in D_2O. Residues with triangles are those with remaining HSQC signals 3 h after dissolution in D_2O. Arrows at the top of the sequence are used to indicate the residues in the β-strands S1, S2, and S3. **B:** Backbone diagram of the β-strands. The antiparallel β-strands are defined by sequential and interstrand backbone NOEs. Thick arrows indicate strong NOEs. Thin arrows indicate medium or weak NOEs. Vertical dashed lines indicate predicted hydrogen bonds derived from the slowly exchanging amide protons and NOE connectivities.

nates of the solution structure of hTFIIB-NTD have been deposited in the RCSB Protein Data Bank (PDB) with accession code 1DL6. The best-fit superposition of the 25 structures along their backbone C′, C^α, and N atoms demonstrates that hTFIIB-NTD forms a well-defined fold in the structural region between residues Thr14–Asp26 and Asp31–Gly42 (Fig. 2A). The mean pairwise RMSDs for backbone and all heavy atoms in this most precisely defined region (Thr14–Asp26 and Asp31–Gly42) are 0.45 ± 0.10 Å and 0.97 ± 0.13 Å, respectively (Table 1). Residues Ala2–Val13, Tyr27–Gly30, and Asp43–Lys59 are disordered in the calculated structures, consistent with their fast exchanging backbone amide protons, relatively few nonsequential NOEs, and the presence of random coil chemical shifts for the assigned amide nitrogens and H^α protons (data not shown).

The three-stranded antiparallel β-sheet formed by residues Leu23–Asp26, Asp31–Cys34, and Leu39–Val41 consists of mostly hydrophobic residues with well-defined side-chain conformations (Figs. 1B, 2A). The hydrophobic residues, namely Leu23, Val24, Met32, Ile33, Leu39, Val40, and Val41, form hydrophobic clusters on the two sides of the β-sheet. Residues Glu25, Asp26, Asp31, and Asp43 form an acidic patch located at one end of the β-sheet and on both faces of the β-sheet. Residues Cys15–His17 form a type I turn (Richardson, 1981) with S^γ of Cys15 and $N^{\delta 1}$ of His17 coordinating to the zinc atom. The other two metal-binding residues Cys34 and Cys37 are located in a typical "rubredoxin" turn (Adman et al., 1975) consisting of six residues from Cys34 to Leu39.

Analysis of the ϕ and ψ angles in the 25 structures using the program PROCHECK-NMR (Laskowski et al., 1996) shows that 51.3% of these angles are in the most favorable region and 95.3% of these angles fall within the allowed regions. The residues with unfavorable conformations fall in the disordered N- and C-terminal regions of the structures. The ϕ and ψ angles of the residues in the well-defined regions of the structures (Thr14–Asp26 and Asp31–

Table 1. *Structural statistics and rmsds for the NMR-derived structures of the hTFIIB-NTD*

	⟨SA⟩[a]
Mean pairwise RMSD[b] (Å) (residues 14–26 and 31–42)	
Backbone (N, C′, and C^{α})	0.45 ± 0.10
All heavy atoms	0.97 ± 0.13
PROCHECK-NMR[c]	
Residues in allowed region of Ramachandran plot (%)	95.3
RMSDs from experimental distance restraints[d] (Å)	
All (443)	0.0106 ± 0.0012
Intraresidue (156)	0.0079 ± 0.0035
Interresidue sequential ($i, i + 1$) (157)	0.0115 ± 0.0037
Interresidue medium ($1 < \|i - j\| \leq 4$) (52)	0.0126 ± 0.0020
Interresidue long ($\|i - j\| \geq 5$) (66)	0.0088 ± 0.0016
Hydrogen bond (12)	0.0132 ± 0.0046
RMSDs from idealized geometry	
Bonds (Å)	0.0014 ± 0.0001
Angles (deg)	0.4545 ± 0.0159
Impropers (deg)	0.1170 ± 0.0130

[a] ⟨SA⟩ is the ensemble of 25 NMR-derived solution structures for hTFIIB-NTD (residues 2–59).

[b] The ensemble was superimposed on N, C′, and C^{α} atoms of residues in the well-defined region of hTFIIB-NTD, comprising residues 14–26 and 31–42.

[c] The PROCHECK-NMR program was used to assess the overall quality of the structures.

[d] The number of each type of distance restraint is given in parentheses. Two distance restraints were imposed per hydrogen bond with bounds of 1.8–2.4 Å (H–O) and 2.7–3.3 Å (N–O). There is no restraint violation greater than 0.2 Å for distance restraints.

Gly42) have lower circular variances and have ϕ and ψ angles characteristic of the secondary structures predicted by the experimental NOE cross peaks. For example, Pro16 and Asn17 in the predicted type I turn have (ϕ, ψ) angles of approximately (−60, −30) and (−90, 0) (Richardson, 1981), respectively. The ϕ and ψ angle values of the residues in the "rubredoxin" turn are close to the ϕ and ψ angle values in the crystal structure of rubredoxin (see Discussion) (Adman et al., 1975; Watenpaugh et al., 1980). The ϕ and ψ angles of the residues in the predicted β-strands are also located in the beta region of the Ramachandran plot. The type of turn in residues His18–Ala21 is not determined due to the variable ϕ and ψ angles of residue Asp20.

Hydrogen-bonding restraints were implemented in the structure calculations to define the β-sheet, but hydrogen bonds were not used for defining other regions of the protein, such as the type I and "rubredoxin" turns. However, N–H–S and N–H–O hydrogen bonds were identified within the type I (residues Cys15–His18) and "rubredoxin" (residues Cys34–Leu39) turns in the final structures (Table 2) (Fig. 2B,C). Within the type I turn, S^{γ} of Cys15 forms a hydrogen bond with the backbone H^N of Asn17. S^{γ} of Cys15 also forms a second hydrogen bond with the backbone H^N of His18. The latter N–H–S hydrogen bond (between H^N of residue $i + 3$ and the side-chain S^{γ} of residue i) is different from the hydrogen-bonding pattern in a typical type I turn, which usually contains a N–H–O hydrogen bond between the backbone H^N of residue $i + 3$ and the carbonyl oxygen of residue i. Within the "rubredoxin" turn, S^{γ} of Cys34 forms the characteristic bifurcated hydrogen bond with the backbone H^Ns of Glu36 and Cys37, and the backbone H^N of Gly38 forms a hydrogen bond with the carbonyl oxygen of Pro35. These hydrogen bonds are usually observed in a typical "rubredoxin" turn (Schwabe & Klug, 1994). The formation of N–H–O and N–H–S hydrogen bonds within the "rubredoxin" and type I turns is consistent with the slowly exchanging amide protons determined by observation of remaining amide cross peaks in a series of ^1H-^{15}N HSQC experiments collected after dissolution in D_2O (Fig. 1A). The slowly exchanging amide proton of Leu39 also suggests the presence of a N–H–S hydrogen bond between H^N of Leu39 and S^{γ} of Cys37, which is expected for a typical "rubredoxin" turn. The average H–S and N–S distances between the backbone amide group of Leu39 and S^{γ} of Cys37 are 3.34 ± 0.13 and 3.87 ± 0.10, respectively. These distances indicate that the backbone amide group of Leu39 is not pointing toward S^{γ} of Cys37 and N–H–S hydrogen bonding is probably not present. The large deviation from linearity of the N, H, and S atoms may also be an artifact caused by insufficient NOE restraints for H^N of Leu39.

Discussion

Comparison with other zinc ribbons

Sequence alignment of the C(H/C)CC motifs of several eucaryal and archaeal TF(II)B proteins indicates a high degree of sequence homology within this family of proteins (Fig. 3A). A superposition of the NMR structures of the zinc ribbons of hTFIIB (residues Cys15–Val41; blue lines in Fig. 3B) and *Pf*TFB (residues Cys7–Ile33; red lines in Fig. 3B) shows that these domains adopt a similar fold, with local structural differences. The β-sheet and the "rubredoxin" turn between β-strands 2 and 3 are very similar between these structures. Hydrophobic residues (leucine, isoleucine, and valine) dominate the composition of the β-strands of both zinc ribbons (Fig. 3A). However, aromatic residues, which are not found in the β-sheet of hTFIIB-NTD, are present in the β-sheet of *Pf*TFB-NTD (Fig. 3A). The third β-strand of hTFIIB-NTD also does not contain the β-bulge observed in *Pf*TFB-NTD and is

Table 2. *N–H–S[a] and N–H–O[b] hydrogen bonds (Å) in the type I and "rubredoxin" turns*

Donor	Acceptor	D–A[c]	H–A
N-H Asn17	S Cys15	3.54 ± 0.08	2.68 ± 0.06
N-H His18	S Cys15	3.29 ± 0.05	2.66 ± 0.09
N-H Glu36	S Cys34	3.59 ± 0.09	2.76 ± 0.20
N-H Cys37[d]	S Cys34	3.82 ± 0.09	2.95 ± 0.12
N-H Gly38	O Pro35	2.73 ± 0.21	2.11 ± 0.23

[a] For N–H–S hydrogen bond, N–S and H–S distances are 3.25–3.55 and 2.3–2.8 Å (Adman et al., 1975).

[b] For N–H–O hydrogen bond, N–O and H–O distances are 2.64–3.04 and 1.75–2.15 Å (Baker & Hubbard, 1984).

[c] A represents S^{γ} and O as the hydrogen-bonding acceptors in N–H–S and N–H–O hydrogen bonds. D represents the backbone N atom.

[d] The N–S and H–S distances are slightly larger than the distances for N–H–S hydrogen bonds. This can be considered as an "incipient" hydrogen bond (Adman et al., 1975).

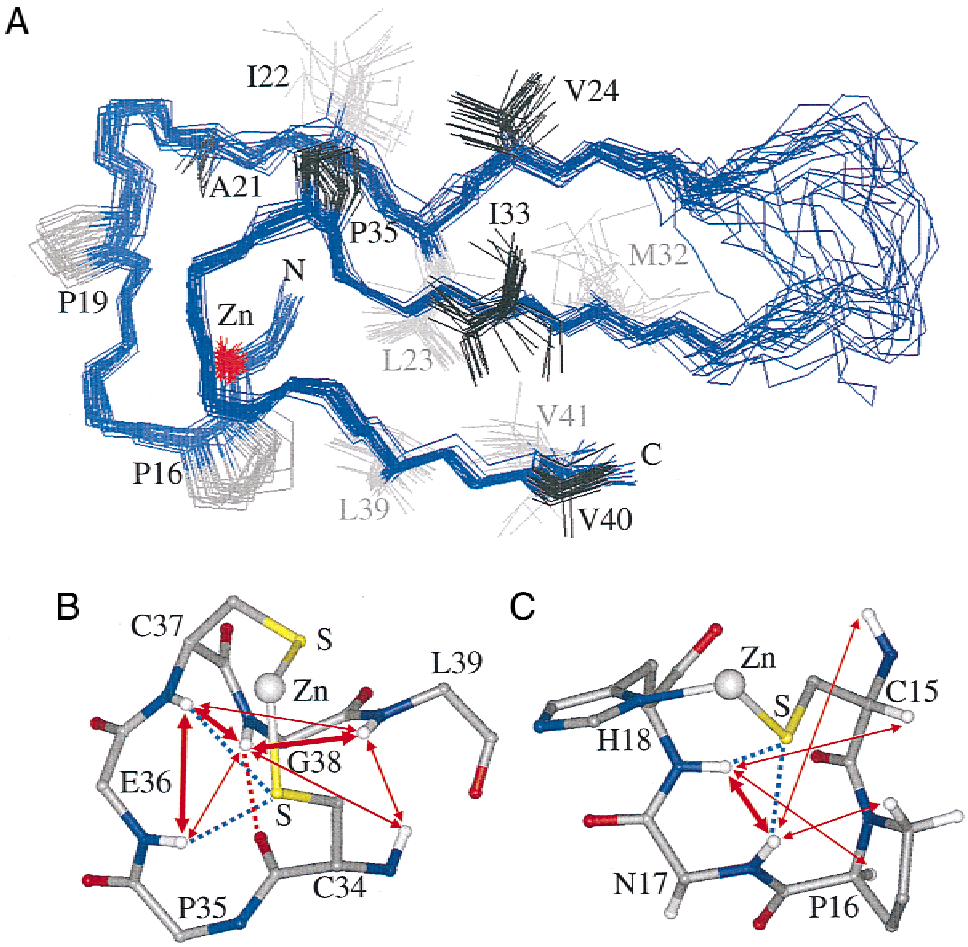

Fig. 2. NMR solution structures of human TFIIB-NTD (PDB ID code 1dl6) and hydrogen bonds and NOE connectivities in the metal-binding turns. **A:** Best-fit superposition of the backbone (N,C^{α},C′; blue) atoms of the well-defined region of the 25 simulated annealing structures (residues 14–41). Hydrophobic side chains are shown in black and gray. Zinc atoms are shown in red. **B:** The hydrogen bonds and NOE connectivities in the "rubredoxin" turn (residues 34–39). **C:** The hydrogen bonds and NOE connectivities in the type I turn (residues 15–17). In **B** and **C**, thick red arrows indicate strong NOEs. Thin red arrows indicate medium or weak NOEs. N–H–S and N–H–O hydrogen bonds are denoted by blue and red dashed lines, respectively. Zinc atom is represented by the gray sphere. Color schemes for atoms in **B** and **C:** carbon, gray; nitrogen, blue; oxygen, red; sulfur, yellow; hydrogen, light gray.

shorter (Leu39–Val41) than that of *Pf* TFB-NTD (Tyr31–Glu35). Gly42 of hTFIIB-NTD (conserved in higher eucaryal TFIIB sequences, Fig. 3A) can adopt a flexible conformation and may disrupt the β-strand formation in hTFIIB-NTD.

Cys34–Leu39 of hTFIIB-NTD and Cys26–Tyr31 of *Pf* TFB-NTD form "rubredoxin" turns, which consist of the CXXCXX metal-binding sequence (Figs. 2B, 3B). The "rubredoxin" turn is stabilized by several H^N–S^{γ} hydrogen bonds within the turn, especially the hydrogen bond between each X-$H^N(i+2)$ and $S^{\gamma}(i)$ (Schwabe & Klug, 1994). The CXXCXX "rubredoxin" turns in the X-ray crystal structures of rubredoxin and several zinc-finger proteins adopt a unique conformation (Adman et al., 1975; Watenpaugh et al., 1980), in which the ϕ and ψ angles of the first cysteine are located in the beta region of the Ramachandran plot, those of the next three residues are located in the alpha region, and the ϕ angle of the fifth residue (after the second cysteine) is positive (approximately 90°). The positive ϕ angle of the fifth residue, which is usually a sterically nonrestricted glycine in many CXXCXX sequences, appears to be essential to stabilize the N–H–S hydrogen bond between H^N of the sixth residue and S^{γ} of the second cysteine (Adman et al., 1975). The second metal-binding sequences of both hTFIIB-NTD and *Pf* TFB-NTD adopt this conserved conformation. The first metal-binding turn of *Pf* TFB-NTD (Fig. 3A) also consists of a CXXCXX module (Cys7–Cys10) and forms a "rubredoxin" turn (Figs. 2B, 3B) (Zhu et al., 1996). In contrast, the first metal-binding turn (Cys15–His18; a CXXH module) of hTFIIB-NTD forms a type I turn (Figs. 2C, 3B). It is interesting to note that this type I turn is stabilized by the bifurcated N–H–S hydrogen bond between S^{γ} of Cys15 and H^Ns of Asn17 and His18 (Fig. 2C), which is unusual for a type I turn and more commonly found in "rubredoxin" turns.

Unlike the well-defined β-turn (Pro19–Gly22) between the first two β-strands of *Pf* TFB-NTD, the homologous residues of hTFIIB-NTD (Tyr27–Gly30) do not adopt a defined conformation (Fig. 3B). Several strong backbone NOE connectivities are present between the residues in the β-turn of *Pf* TFB-NTD, while the backbone NOE connectivities for the corresponding residues in hTFIIB-NTD are mostly weak. The rigid-ring structure of Pro19 of *Pf* TFB-

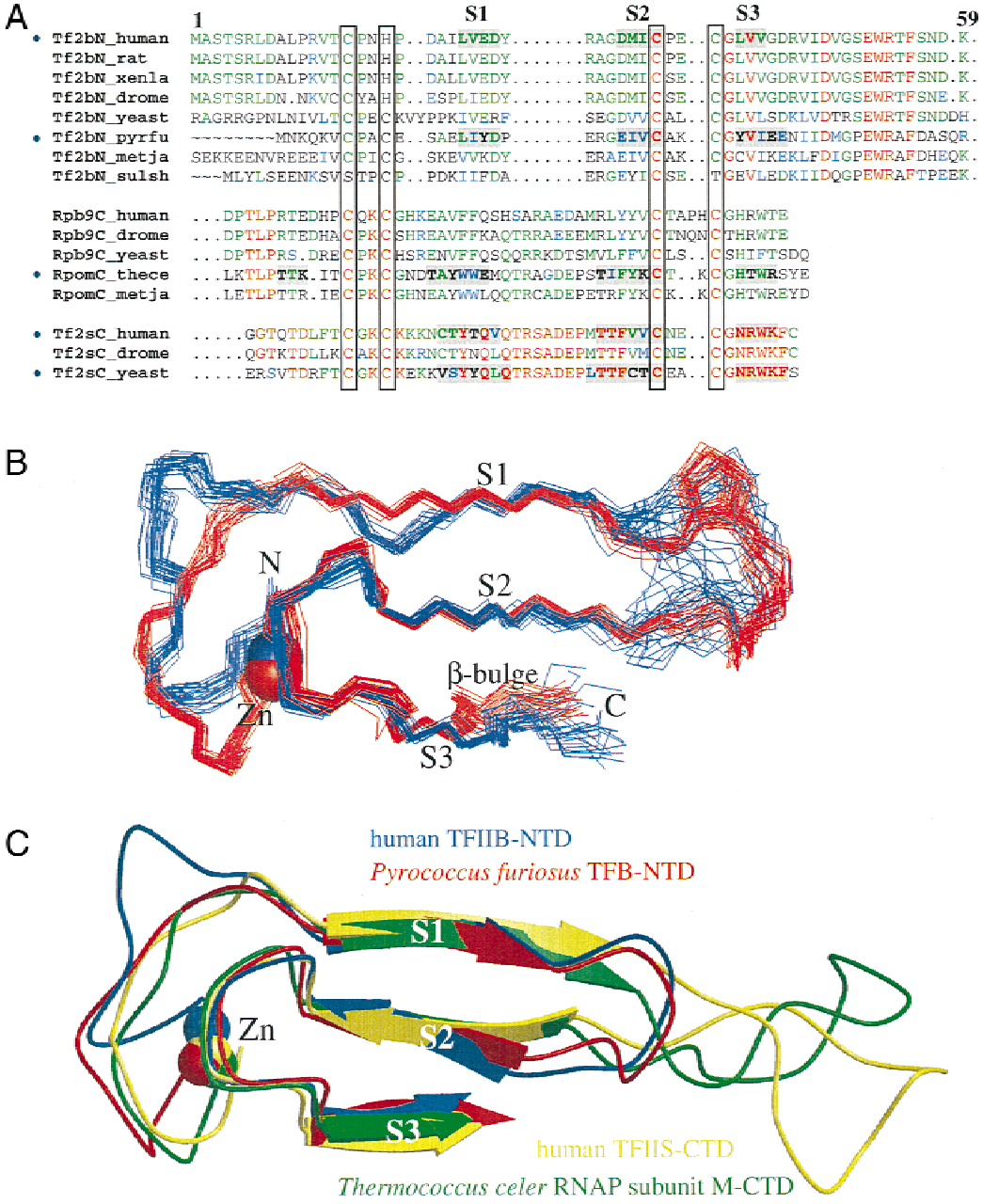

Fig. 3. Sequence alignment of zinc-ribbon motifs and comparison of zinc ribbon structures. **A:** Comparison of the sequences of the N-terminal domain of TF(II)B (Tf2bN), the C-terminal domain of RNAPII subunit 9 (subunit M in archaea) (Rpb9C or RpomC), and the C-terminal domain of TFIIS (Tf2sC). Cysteines and histidines proposed to coordinate zinc are aligned in vertical boxes. Blue solid circles on the left indicate sequences for which 3D structures have been determined. The β-strands of the zinc ribbons are highlighted with gray bars. Conservation is indicated as follows: red text, completely conserved; green text, conserved in half or more than half of the amino acid sequences; blue text, similar to the conserved amino acid residues. Abbreviations: xenla, *Xenopus laevis*; drome, *Drosophila melanogaster*; yeast, *Saccharomyces cerivisiae*; pyrfu, *Pyrococcus furiosus*; metja, *Methanococcus jannaschii*; sulsh, *Sulfolobus shibatae*; thece, *Thermococcus celer*. **B:** Comparison of the solution structures of hTFIIB-NTD (blue) and *Pf* TFB-NTD (red). Only the backbone C′, C^{α}, and N atoms in the well-defined regions of the two proteins (Cys15–Val41 of hTFIIB-NTD and Cys7–Glu35 of *Pf* TFB-NTD) are shown in the superposition of 25 structures from each protein. The superposition was obtained by the least-squares fit of the backbone atoms of the residues in the β-sheet and the "rubredoxin" turn, including Cys15–Pro16, Ile22–Asp26, and Asp31–Val41 of hTFIIB-NTD and Cys7–Pro8, Glu14–Asp18, and Glu23–Ile33 of *Pf* TFB-NTD. The mean pairwise backbone RMSD of the superimposed residues is 1.0 Å. Approximate positions of the zinc atoms in the structures are displayed in red sphere for the zinc atoms in hTFIIB-NTD and in white sphere for those in *Pf* TFB-NTD. **C:** Comparison of zinc ribbon structures, obtained by best-fit superposition of the backbone C′, C^{α}, and N atoms of the three β-strands (S1, S2, and S3) and the "rubredoxin" turn between strand 2 and strand 3. Each zinc ribbon is displayed by the backbone trace (lines for coils and turns and planar arrows for β-strands) from the first metal-binding cysteine to the last residue in the third β-strand. The zinc atom in each structure is shown as a solid sphere with the same color as the backbone trace. Sequences used for the superposition are: Leu23–Asp26 and Asp31–Val41 of hTFIIB-NTD (blue), Leu15–Asp18 and Glu23–Ile33 of *Pf* TFB-NTD (red), Cys271–Thr274 and Phe288–Trp298 of hTFIIS-CTD (yellow-green), and Ala79–Trp82 and Phe96–Trp106 of *Tc*RNAP subunit M-CTD (green). The mean pairwise backbone RMSD of the superimposed residues is 1.0 Å. The structure (one for each zinc ribbon) with the lowest backbone RMSD from the mean coordinates of each structural ensemble was selected for the comparison. The PDB ID codes for the zinc ribbons are: 1dl6, hTFIIB-NTD; 1pft, *Pf* TFB-NTD; 1tfi, hTFIIS-CTD; 1qyp, *Tc*RNAP subunit M-CTD.

NTD (Fig. 3B) may contribute to the stability of the β-turn, as may the global stability of the β-sheet.

A superposition of the zinc ribbons of hTFIIB-NTD, *Pf*TFB-NTD (Zhu et al., 1996), hTFIIS-CTD (Qian et al., 1993), and the C-terminal domain of *Thermococcus celer* RNA polymerase subunit M (*Tc*RNAP subunit M-CTD, RPB9 in eucarya) (Wang et al., 1998) is shown in Figure 3C. Except for an additional β-strand (not shown in Fig. 3C) N-terminal to the first metal-binding cysteine in the zinc ribbon of *Tc*RNAP subunit M-CTD, the secondary structure elements of each zinc ribbon comprise two metal-binding turns and three antiparallel β-strands. The best-fit superposition along the β-strands and the second metal binding turn (the "rubredoxin" turn) of each zinc ribbon gives a mean pairwise RMSD of 1.0 Å for superimposed backbone atoms, suggesting that these elements are essential for formation of a "zinc ribbon." Sequences homologous to these C(H/C)CC metal-binding motifs are also present in other transcription-related factors such as subunits 2 and 12 of RNA pol II (Wang et al., 1998) and TFIIE (Qian et al., 1993). They have been found in bacteriophage T4 and T7 primases (Qian et al., 1993), which are both involved in DNA replication. Currently, it is not known what direct role the zinc ribbon structural motif plays in transcription. Biochemical studies of TFIIS and primases have implicated the involvement of protein domains including the zinc ribbon motif in protein–nucleic acid interactions (Agarwal et al., 1991; Kusakabe et al., 1999). The zinc ribbon motif in TFIIB may also be involved in protein–nucleic acid interactions in the PIC, although the low content of aromatic and basic residues indicates otherwise (Fig. 3A). Another possible role of the TF(II)B zinc ribbon involves protein–protein interactions with other transcription factors in the PIC. Indeed, as discussed below, other work has suggested the involvement of the TFIIB zinc ribbon in interactions with the GTFs, RNA pol II, and other transcription-related proteins.

Involvement of the N-terminal domain of TFIIB in PIC formation

The N-terminal domain of TFIIB has been implicated in both basal and regulated transcription initiation. The molecular mechanism of TFIIB-NTD's involvement in PIC formation is possibly through contacts between the zinc ribbon and the RNA pol II/TFIIF complex (Tschochner et al., 1992; Barberis et al., 1993; Buratowski & Zhou, 1993; Ha et al., 1993; Hisatake et al., 1993; Malik et al., 1993; Bushnell et al., 1996; Fang & Burton, 1996; Bangur et al., 1997; Lin et al., 1997). With the structure of hTFIIB-NTD in hand, we can map the results of mutagenesis experiments onto the zinc ribbon structural elements. In vitro transcription assays using N-terminal deletion mutants of TFIIB showed that the residues before Cys15 are not required for full transcriptional activity (Hisatake et al., 1993; Yamashita et al., 1993). Further deletion of the N-terminus before the first β-strand (through Ala21) and mutations of the metal-binding residues conferred a reduced level of transcriptional activity (Buratowski & Zhou, 1993). Deletions involving any residues in the β-strands of the zinc ribbon resulted in complete loss of transcriptional activity (Hisatake et al., 1993). Point mutations of the last two cysteines and residues in the third β-strand of the zinc ribbon also impair stable RNA pol II binding and cause a reduced level of transcriptional activity (Bangur et al., 1997; Pardee et al., 1998; Wu & Hampsey, 1999). In summary, these studies indicate that an intact β-sheet structure is essential for transcriptional activity and binding to RNA pol II/TFIIF. Because deletion of the first metal-binding loop (Cys15–His18 in hTFIIB) did not completely eliminate but reduced transcriptional activity, we suggest that an intact metal binding site stabilizes the β-sheet, which may form the essential element for interaction with other components of the PIC.

Conclusions

The close relationship between Archaea and Eucarya is reflected most strongly in information-processing genes (Bult et al., 1996). In the transcriptional apparatus, sequence homology is mirrored by structural similarity in the TATA-binding protein (TBP) and in the C-terminal core domain of transcription factor (TF) IIB (Thomm, 1996). The N-terminal domain of TFIIB, recognized for linking the promoter-recognition machinery (TATA box-TBP) to the catalytic machinery (RNA polymerase II) (Ha et al., 1993), was structurally characterized first from an archaeal source and exhibited a zinc ribbon structure featuring a $Zn(Cys)_4$ metal-binding site. Higher eucaryal versions of this domain involve a replacement of the second Cys with His, raising the question of whether this Cys-His-Cys-Cys sequence motif would also fold to a zinc ribbon structure. The work described herein confirms that this occurs, identifying this zinc ribbon structural motif as a highly conserved structure throughout the evolution of transcription in the Archaea-Eucarya branch.

Materials and methods

Protein expression and purification

Plasmid containing the gene for full-length hTFIIB was generously provided by D. Reinberg. DNA coding for the first 59 residues of hTFIIB was subcloned into bacterial expression vector pT7-7. The plasmid was transformed into *Escherichia coli* BL-21 DE3 cells. The transformed *E. coli* cells were grown at 37 °C in M9 media with glucose (4 g/L) and ammonium chloride (1 g/L) as the sole carbon and nitrogen sources, respectively. Cells were grown to an optical density (OD_{600}) of about 0.9 and subsequently induced with 0.1 mM (final concentration) isopropyl β-D-thiogalactopyranoside (IPTG). Along with the addition of IPTG, zinc sulfate and ferrous ammonium sulfate were added to final metal concentrations of 0.087 mM zinc and 0.013 mM iron. The culture was grown an additional 4 h ($OD_{600} \sim 2.0$) and harvested by low-speed centrifugation. Cell pellets were frozen and stored at −80 °C until they were used. ^{15}N-labeled hTFIIB-NTD was expressed from media containing ^{15}N-labeled ammonium chloride.

Cell paste (10–12 g) from a 4 L growth was thawed by suspension in 60 mL lysis buffer (50 mM potassium phosphate pH 7.0, 10 mM 2-mercaptoethanol, 1 mM phenylmethanesulfonyl fluoride (PMSF), 1 μg/mL leupeptin, and 1 μg/mL DNase I). The cells were lysed by sonication and the supernatant was clarified by centrifugation at 30,000 × *g* for 50 min at 4 °C. The supernatant was loaded onto a 2.5 × 10 cm QAE-sephadex G-25 column (Pharmacia, Uppsala, Sweden) and washed extensively with 50 mM potassium phosphate buffer, pH 7.0. The hTFIIB-NTD protein was eluted between 200 and 300 mM potassium chloride in 50 mM potassium phosphate pH 7.0. The eluate was desalted and concentrated using an Amicon ultrafiltration unit (Amicon, Beverly, Massachusetts) fitted with a YM3 membrane. The resulting sample was ~90% hTFIIB-NTD by SDS-PAGE. Further purification by

Mono-Q (HR 10/10; Pharmacia) chromatography was performed on an FPLC system (Pharmacia) using a 60 mL linear gradient from 100 to 400 mM potassium chloride in 25 mM potassium phosphate, pH 7.0. Pooled fractions containing hTFIIB-NTD (eluted at about 300 mM potassium chloride) were desalted and concentrated to ~1 mM using an Amicon ultrafiltration unit with a YM3 membrane. The sample was then transferred to a Centricon3 ultrafiltration cell and concentrated to about 15 mM hTFIIB-NTD in 25 mM potassium phosphate pH 7.0. The concentrated protein sample was stored at −80 °C until it was used for NMR studies. The concentration of hTFIIB-NTD was determined either by quantitative protein assay (Coomassie Plus; Pierce, Rockford, Illinois) or using an extinction coefficient at 280 nm of 7,150 L mol^{-1} cm^{-1} calculated on the basis of the amino acid composition (Pace et al., 1995). The resulting hTFIIB-NTD sample was ~95% pure by SDS-PAGE. Typically, the yield was about 40 mg of pure hTFIIB-NTD per liter of minimal medium.

Electrospray ionization mass spectrometry of the resulting sample revealed a single molecular ion series with a deconvoluted mass of 6361 amu, corresponding to hTFIIB-NTD without the N-terminal methionine (calculated mass 6,362 amu). The metal content of the resulting sample was measured by inductively coupled plasma atomic emission spectroscopy (ICP-AES) in the Chemical Analysis Laboratory at the University of Georgia. The stoichiometry of zinc with respect to polypeptide chain was determined to be 0.98 ± 0.02 zinc atom per hTFIIB-NTD polypeptide chain.

NMR spectroscopy

NMR samples of hTFIIB-NTD contained protein concentrations of 2–3 mM in the following buffer: 25 mM potassium phosphate, pH 7.0, with 10% (v/v) D_2O. All NMR data were obtained at 25 °C with a Varian ^{unity}*INOVA* 600 MHz spectrometer (Varian, Palo Alto, California) equipped with an actively shielded z gradient HCN triple resonance probe and a pulse field gradient (PFG) driver. NMR data were processed using the Varian software or NMRPipe (Delaglio et al., 1995) and analyzed with NMRDraw (version 1.7). The following ^{1}H homonuclear 2D experiments were performed: DQF-COSY (Rance et al., 1983), TOCSY (mixing time 50 ms) (Bax & Davis, 1985), and NOESY (mixing times 100, 150, and 200 ms) (Jeener et al., 1979). In each of these cases, water suppression was achieved by solvent presaturation. Acquisition times (57.3 ms in t_1 for 512 complex points and 147 ms in t_2 for 1,024 complex points) were the same for each homonuclear experiment. Heteronuclear spectra were collected on a uniformly ^{15}N-labeled protein sample. PFGs were employed to suppress spectral artifacts, to minimize the water signal, and for coherence transfer selection. A ^{1}H-^{15}N heteronuclear single-quantum coherence (HSQC) (Kay et al., 1992) spectrum was obtained with a t_1 acquisition time of 116 ms (256 complex points) and a t_2 acquisition time of 128 ms (1,024 complex points). A ^{1}H-^{15}N HSQC-TOCSY (mixing time 50 ms) (Marion et al., 1989) spectrum was acquired with a t_1 acquisition time of 116 ms (256 complex points) and a t_2 acquisition time of 147 ms (1,024 complex points). A 3D ^{15}N edited NOESY-HSQC (Zhang et al., 1994) spectrum was collected at a mixing time of 150 ms. The spectral parameters included a t_1 acquisition time of 16 ms for the indirect ^{1}H dimension (128 complex points), a t_2 acquisition time of 14.6 ms for the ^{15}N dimension (32 complex points), and a t_3 acquisition time of 128 ms for the directly observed ^{1}H dimension (1,024 complex points). To characterize backbone amide protons that exchange slowly with the solvent, the ^{15}N-labeled protein was lyophilized and redissolved in D_2O, and a series of ^{1}H-^{15}N HSQC spectra (50 ms in t_1, 64 ms in t_2) were obtained every 15 min for 3 h after dissolution in D_2O.

Structure calculation and molecular modeling

Three-dimensional structures were calculated with a distance geometry/simulated annealing (DG/SA) protocol using the CNS program (Brünger et al., 1998). Approximate interproton distance restraints were derived from the multidimensional NOESY spectra. NOEs were grouped into four distance ranges, 1.8–2.7 Å (1.8–2.9 Å for NOEs involving NH protons), 1.8–3.3 Å (1.8–3.5 Å for NOEs involving NH protons), 1.8–5.0 Å, and 1.8–6.0 Å, corresponding to strong, medium, weak, and very weak NOE intensities, respectively. An additional 0.5 Å was applied to the upper distance limits for NOEs involving methyl protons. Stereospecific assignments for methylenes were not obtained, and pseudo-atoms located at the midpoints between pairs of nuclei were used for assignments of distance restraints. Hydrogen bonds were included as distance restraints and given bounds of 1.8–2.4 Å (H–O) and 2.7–3.3 Å (N–O) for each hydrogen bond. Determination of hydrogen bonds in the β-sheet region was based on the long-range NOEs (see Results) and the slow-exchanging amide protons. The structure calculation employed 431 proton/proton distance restraints from NOE data and 12 hydrogen-bonding restraints. In the first stage of the calculation an initial ensemble of 200 structures was generated from a single covalent structure with randomized backbone dihedral angles and extended side chains using a DG protocol followed by restrained SA. Only 28 structures generated from DG/SA had no restraint violation greater than 0.5 Å and were selected for further SA refinement. Hydrogen-bonding restraints and appropriate covalent restraints for the tetrahedral (Cys_3His) zinc center (Omichinski et al., 1990) were introduced during the second stage of refinement using a torsion-angle molecular dynamics protocol (Rice & Brünger, 1994; Stein et al., 1997). Covalent restraints for the (Cys_3His) zinc center were obtained from the mean values of the bond lengths and bond angles measured in two inorganic compounds with tetrahedral (S_3N) zinc centers (Cambridge Structure Database, CSD codes: ZAZQUM and SEJZOW). The covalent restraints for the (Cys_3His) zinc center consisted of bond lengths of 2.3 and 2.0 Å for the Cys S^γ-Zn and His $N^\delta1$-Zn bonds, respectively, and bond angles of 108 and 126° for Cys C^β-Cys S^γ-Zn and His C^γ-His $N^\delta1$-Zn, respectively. In addition, an improper angle of 0° was employed for Zn-His C^γ-His $C^\epsilon1$-His $N^\delta1$ to ensure that the zinc is in the same plane as the His ring. Bond angles of 113.8 and 104.9° for Cys S^γ-Zn-Cys S^γ and Cys S^γ-Zn-His $N^\delta1$, respectively, were also applied for maintaining the tetrahedral geometry of the zinc center. The weights for the Cys S^γ-Zn-Cys S^γ and Cys S^γ-Zn-His $N^\delta1$ energy terms were one-fifth that of the regular bond angles. An ensemble of 25 lowest energy structures with no restraint violations greater than 0.2 Å was selected for structural visualization and analyzed using InsightII (MSI, San Diego, California), Molmol (Koradi et al., 1996), MOLSCRIPT (Kraulis, 1991), and PROCHECK-NMR (Laskowski et al., 1996) programs. The structure with the lowest RMS derivation from the mean coordinates of the 25 structures was selected for structural comparison with other zinc ribbon motifs.

Acknowledgment

We thank Dr. L.E. Kay for NMR pulse sequences. H.-T. Chen thanks Dr. Q. Teng for assistance with NMR measurements and processing,

Dr. M.W.F. Fischer for assistance with structure calculations, and Dr. J.H. Prestegard for useful discussions. This work was supported by the National Science Foundation (MCB 96-31093 to RAS). NMR instrumentation and operation are partially supported by the Georgia Research Alliance Biotechnology Center and by the UGA Structural Biology Initiative.

References

Adman E, Watenpaugh KD, Jensen LH. 1975. NH–S hydrogen bonds in *Peptococcus aerogenes* ferredoxin, *Clostridium pasteurianum* rubredoxin, and Chromatium high potential iron protein. *Proc Natl Acad Sci USA 72*:4854–4858.

Agarwal K, Baek KH, Jeon CJ, Miyamoto K, Ueno A, Yoon HS. 1991. Stimulation of transcript elongation requires both the zinc finger and RNA polymerase II binding domains of human TFIIS. *Biochemistry 30*:7842–7851.

Bagby S, Kim S, Maldonado E, Tong KI, Reinberg D, Ikura M. 1995. Solution structure of the C-terminal core domain of human TFIIB: Similarity to cyclin A and interaction with TATA-binding protein. *Cell 82*:857–867.

Baker EN, Hubbard RE. 1984. Hydrogen bonding in globular proteins. *Prog Biophys Mol Biol 44*:97–179.

Bangur CS, Pardee TS, Ponticelli AS. 1997. Mutational analysis of the D1/E1 core helices and the conserved N-terminal region of yeast transcription factor IIB (TFIIB): Identification of an N-terminal mutant that stabilizes TATA-binding protein-TFIIB-DNA complexes. *Mol Cell Biol 17*:6784–6793.

Barberis A, Muller CW, Harrison SC, Ptashne M. 1993. Delineation of two functional regions of transcription factor TFIIB. *Proc Natl Acad Sci USA 90*:5628–5632.

Bax A, Davis DG. 1985. MLEV-17-based two-dimensional homonuclear magnetization transfer spectroscopy. *J Magn Reson 65*:355–360.

Brünger AT, Adams PD, Clore GM, DeLano WL, Gros P, Grosse-Kunstleve RW, Jiang JS, Kuszewski J, Nilges M, Pannu NS, et al. 1998. Crystallography & NMR system: A new software suite for macromolecular structure determination. *Acta Crystallogr D Biol Crystallogr 54*:905–921.

Bult CJ, White O, Olsen GJ, Zhou L, Fleischmann RD, Sutton GG, Blake JA, FitzGerald LM, Clayton RA, Gocayne JD, et al. 1996. Complete genome sequence of the methanogenic archaeon, *Methanococcus jannaschii*. *Science 273*:1058–1073.

Buratowski S, Zhou H. 1993. Functional domains of transcription factor TFIIB. *Proc Natl Acad Sci USA 90*:5633–5637.

Bushnell DA, Bamdad C, Kornberg RD. 1996. A minimal set of RNA polymerase II transcription protein interactions. *J Biol Chem 271*:20170–20174.

Clore GM, Gronenborn AM. 1989. Determination of three-dimensional structures of proteins and nucleic acids in solution by nuclear magnetic resonance spectroscopy. *Crit Rev Biochem Mol Biol 24*:479–564.

Colangelo CM, Lewis LM, Cosper NJ, Scott RA. 2000. Structural evidence for a common zinc binding domain in archaeal and eucaryal transcription factor IIB proteins. *J Biol Inorg Chem 5*:276–283.

Cramer P, Bushnell DA, Fu J, Gnatt AL, Maier-Davis B, Thompson NE, Burgess RR, Edwards AM, David PR, Kornberg RD. 2000. Architecture of RNA polymerase II and implications for transcription mechanism. *Science 288*:640–649.

Delaglio F, Grzesiek S, Vuister GW, Zhu G, Pfeifer J, Bax A. 1995. NMRPipe: A multidimensional spectral processing system based on UNIX pipes. *J Biomol NMR 6*:277–293.

Fang SM, Burton ZF. 1996. RNA polymerase II-associated protein (RAP) 74 binds transcription factor (TF) IIB and blocks TFIIB-RAP30 binding. *J Biol Chem 271*:11703–11709.

Fourmy D, Dardel F, Blanquet S. 1993. Methionyl-tRNA synthetase zinc binding domain. Three-dimensional structure and homology with rubredoxin and gag retroviral proteins. *J Mol Biol 231*:1078–1089.

Ha I, Roberts S, Maldonado E, Sun X, Kim LU, Green M, Reinberg D. 1993. Multiple functional domains of human transcription factor IIB: Distinct interactions with two general transcription factors and RNA polymerase II. *Genes Dev 7*:1021–1032.

Halkides CJ, Wu YQ, Murray CJ. 1996. A low-barrier hydrogen bond in subtilisin: ^{1}H and ^{15}N NMR studies with peptidyl trifluoromethyl ketones. *Biochemistry 35*:15941–15948.

Hampsey M. 1998. Molecular genetics of the RNA polymerase II general transcriptional machinery. *Microbiol Mol Biol Rev 62*:465–503.

Hawkes NA, Roberts SG. 1999. The role of human TFIIB in transcription start site selection in vitro and in vivo. *J Biol Chem 274*:14337–14343.

Hisatake K, Roeder RG, Horikoshi M. 1993. Functional dissection of TFIIB domains required for TFIIB-TFIID-promoter complex formation and basal transcription activity. *Nature 363*:744–747.

Jeener J, Meier BH, Bachmann P, Ernst RR. 1979. Investigation of exchange processes by two-dimensional NMR spectroscopy. *J Chem Phys 71*:4546–4533.

Kay LE, Keifer P, Saarinen T. 1992. Pure absorption gradient enhanced heteronuclear single quantum correlation spectroscopy with improved sensitivity. *J Am Chem Soc 114*:10663–10665.

Koradi R, Billeter M, Wüthrich K. 1996. MOLMOL: A program for display and analysis of macromolecular structures. *J Mol Graph 14*:51–55.

Kraulis PJ. 1991. MOLSCRIPT: A program to produce both detailed and schematic plots of protein structures. *J Appl Crystallogr 24*:946–950.

Kusakabe T, Hine AV, Hyberts SG, Richardson CC. 1999. The Cys4 zinc finger of bacteriophage T7 primase in sequence-specific single-stranded DNA recognition. *Proc Natl Acad Sci USA 96*:4295–4300.

Laskowski RA, Rullmannn JA, MacArthur MW, Kaptein R, Thornton JM. 1996. AQUA and PROCHECK-NMR: Programs for checking the quality of protein structures solved by NMR. *J Biomol NMR 8*:477–486.

Lin Y, Nomura T, Cheong J, Dorjsuren D, Iida K, Murakami S. 1997. Hepatitis B virus X protein is a transcriptional modulator that communicates with transcription factor IIB and the RNA polymerase II subunit 5. *J Biol Chem 272*:7132–7139.

Malik S, Lee DK, Roeder RG. 1993. Potential RNA polymerase II-induced interactions of transcription factor TFIIB. *Mol Cell Biol 13*:6253–6259.

Marion D, Driscoll PC, Kay LE, Wingfield PT, Bax A, Gronenborn AM, Clore GM. 1989. Overcoming the overlap problem in the assignment of ^{1}H NMR spectra of larger proteins by use of three-dimensional heteronuclear ^{1}H-^{15}N Hartmann-Hahn-multiple quantum coherence and nuclear Overhauser-multiple quantum coherence spectroscopy: Application to interleukin 1 beta. *Biochemistry 28*:6150–6156.

Myer VE, Young RA. 1998. RNA polymerase II holoenzymes and subcomplexes. *J Biol Chem 273*:27757–27760.

Nikolov DB, Chen H, Halay ED, Usheva AA, Hisatake K, Lee DK, Roeder RG, Burley SK. 1995. Crystal structure of a TFIIB-TBP-TATA-element ternary complex. *Nature 377*:119–128.

Ohkuma Y, Sumimoto H, Hoffmann A, Shimasaki S, Horikoshi M, Roeder RG. 1991. Structural motifs and potential sigma homologies in the large subunit of human general transcription factor TFIIE. *Nature 354*:398–401.

Olmsted VK, Awrey DE, Koth C, Shan X, Morin PE, Kazanis S, Edwards AM, Arrowsmith CH. 1998. Yeast transcript elongation factor (TFIIS), structure and function. I: NMR structural analysis of the minimal transcriptionally active region. *J Biol Chem 273*:22589–22594.

Omichinski JG, Clore GM, Appella E, Sakaguchi K, Gronenborn AM. 1990. High-resolution three-dimensional structure of a single zinc finger from a human enhancer binding protein in solution. *Biochemistry 29*:9324–9334.

Orphanides G, Lagrange T, Reinberg D. 1996. The general transcription factors of RNA polymerase II. *Genes Dev 10*:2657–2683.

Pace CN, Vajdos F, Fee L, Grimsley G, Gray T. 1995. How to measure and predict the molar absorption coefficient of a protein. *Protein Sci 4*:2411–2423.

Pardee TS, Bangur CS, Ponticelli AS. 1998. The N-terminal region of yeast TFIIB contains two adjacent functional domains involved in stable RNA polymerase binding and transcription start site selection. *J Biol Chem 273*:17859–17864.

Perez-Alvarado GC, Miles C, Michelsen JW, Louis HA, Winge DR, Beckerle MC, Summers MF. 1994. Structure of the carboxy-terminal LIM domain from the cysteine rich protein CRP. *Nat Struct Biol 1*:388–398.

Peterson MG, Inostroza J, Maxon ME, Flores O, Admon A, Reinberg D, Tjian R. 1991. Structure and functional properties of human general transcription factor IIE. *Nature 354*:369–373.

Pinto I, Ware DE, Hampsey M. 1992. The yeast SUA7 gene encodes a homolog of human transcription factor TFIIB and is required for normal start site selection in vivo. *Cell 68*:977–988.

Pinto I, Wu W-H, Na JG, Hampsey M. 1994. Characterization of *sua7* mutations defines a domain of TFIIB involved in transcription start site selection in yeast. *J Biol Chem 269*:30569–30573.

Qian X, Gozani SN, Yoon H, Jeon C, Agarwal K, Weiss MA. 1993. Novel zinc finger motif in the basal transcription machinery: Three-dimensional NMR studies of the nucleic acid binding domain of transcription elongation factor TFIIS. *Biochemistry 32*:9944–9959.

Rance M, Sørensen OW, Bodenhausen G, Wagner G, Ernst RR, Wüthrich K. 1983. Improved spectral resolution in COSY ^{1}H NMR spectra of proteins via double quantum filtering. *Biochem Biophys Res Commun 117*:458–479.

Rice LM, Brünger AT. 1994. Torsion angle dynamics: Reduced variable conformational sampling enhances crystallographic structure refinement. *Proteins 19*:277–290.

Richardson JS. 1981. The anatomy and taxonomy of protein structure. *Adv Protein Chem 34*:167–339.

Roberts SG, Green MR. 1994. Activator-induced conformational change in general transcription factor TFIIB. *Nature 371*:717–720.

Schwabe JW, Klug A. 1994. Zinc mining for protein domains. *Nat Struct Biol 1*:345–349.

Stein EG, Rice LM, Brünger AT. 1997. Torsion-angle dynamics as a new efficient tool for NMR structure calculations. *J Magn Reson 124*:154–164.

Summers MF, South TL, Kim B, Hare DR. 1990. High-resolution structure of an HIV zinc fingerlike domain via a new NMR-based distance geometry approach. *Biochemistry 29*:329–340.

Thomm M. 1996. Archaeal transcription factors and their role in transcription initiation. *FEMS Microbiol Rev 18*:159–171.

Tschochner H, Sayre MH, Flanagan PM, Feaver WJ, Kornberg RD. 1992. Yeast RNA polymerase II initiation factor e: Isolation and identification as the functional counterpart of human transcription factor IIB. *Proc Natl Acad Sci USA 89*:11292–11296.

Wang B, Jones DN, Kaine BP, Weiss MA. 1998. High-resolution structure of an archaeal zinc ribbon defines a general architectural motif in eukaryotic RNA polymerases. *Structure 6*:555–569.

Watenpaugh KD, Sieker LC, Jensen LH. 1980. Crystallographic refinement of rubredoxin at 1.2 Å resolution. *J Mol Biol 138*:615–633.

Wu WH, Hampsey M. 1999. An activation-specific role for transcription factor TFIIB in vivo. *Proc Natl Acad Sci USA 96*:2764–2769.

Wüthrich K. 1986. *NMR of proteins and nucleic acids*. New York: Wiley.

Yamashita S, Hisatake K, Kokubo T, Doi K, Roeder RG, Horikoshi M, Nakatani Y. 1993. Transcription factor TFIIB sites important for interaction with promoter-bound TFIID. *Science 261*:463–466.

Zhang O, Kay LE, Olivier JP, Forman-Kay JD. 1994. Backbone ^{1}H and ^{15}N resonance assignments of the N-terminal SH3 domain of drk in folded and unfolded states using enhanced-sensitivity pulsed field gradient NMR techniques. *J Biomol NMR 4*:845–858.

Zhu W, Zeng Q, Colangelo CM, Lewis LM, Summers MF, Scott RA. 1996. The N-terminal domain of TFIIB from *Pryococcus furiosus* forms a zinc ribbon. *Nat Struct Biol 3*:122–124.